Research Square

Preprints are preliminary reports that have not undergone peer review.
They should not be considered conclusive, used to inform clinical practice,
or referenced by the media as validated information.

Influence of Initial Gas Pressure on the Spatial Intensity Distribution of Double-Pass Amplified 69.8 nm and 72.6 nm Lasers

Shuisen Jiang
Quanzhou Normal University
Tao Liu
Civil Aviation University of China
Huaiyu Cui
Harbin Institute of Technology
Dongdi Zhao
Harbin Institute of Technology
Yongpeng Zhao
zhaoyp3@hit.edu.cn

Harbin Institute of Technology

Research Article

Keywords: Extreme ultraviolet (EUV) laser, Capillary discharge, Double-pass amplification, 69.8 nm, 46.9 nm

Posted Date: November 2nd, 2026

DOI: https://doi.org/10.21203/rs.3.rs-11350896/v1

License: This work is licensed under a Creative Commons Attribution 4.0 International License.
Read Full License

Additional Declarations: No competing interests reported.

Abstract

In this study, a discharge-produced plasma was utilized as the gain medium, and a silicon carbide (SiC) mirror was employed to achieve simultaneous double-pass amplification of Ne-like Ar lasers at 69.8 nm and 72.6 nm. Notably, the double-pass amplification of the 72.6 nm Ne-like Ar laser is reported for the first time in this work. We experimentally investigate the dependence of the spatial intensity distribution of the double-pass amplified 69.8 nm and 72.6 nm lasers on the initial gas pressure. As the gas pressure increases from 14 Pa to 18 Pa, the intensity profile of the double-pass amplified laser evolves from a central-intensity-dominated distribution to an edge-enhanced annular distribution. For the double-pass amplified 69.8 nm laser, the divergence angle increases from 2.1 mrad to a peak-to-peak value of 3.5 mrad. Correspondingly, the divergence angle of the double-pass amplified 72.6 nm laser increases from 1.7 mrad to a peak-to-peak divergence angle of 3.4 mrad.

1. Introduction

Extreme-ultraviolet (EUV) lasers can be generated through energy-level transitions of highly charged ions. Consequently, their gain media consist of high-temperature, high-density plasmas produced by high-energy lasers or high-current discharges. Due to the fact that the bombardment of plasma can easily damage the EUV mirrors, this type of laser generally operates in a single-pass amplification mode. Positioning a reflecting mirror at one end of the plasma to achieve double-pass laser amplification facilitates efficient extraction of the stored energy from the gain medium and yields higher-energy laser output [1]. In EUV laser experiments utilizing high-energy laser-produced plasma as the gain medium, multiple research groups have realized double-pass amplification of EUV lasers with Mo/Si multilayer mirrors [1–4]. A single bombardment from the plasma is sufficient to damage the multilayer mirror, which renders it challenging to quantify the influence of experimental parameters on double-pass amplified lasers. In experimental investigations of EUV lasers utilizing high-current discharge-produced plasmas as gain media, a research group in the United States realized double-pass amplification of the 46.9 nm Ne-like Ar laser with a planar iridium mirror, and successfully achieved gain saturation for this laser system [5]. Nevertheless, a significant reduction in the reflectance of the iridium mirror was observed under bombardment by the plasma generated by three consecutive discharges. Accordingly, mitigating plasma-bombardment-induced damage to the reflectors is a prerequisite for investigating the dependence of double-pass amplified laser output on experimental parameters. Double-pass amplification of Ne-like Ar lasers at 69.8 nm [6] and 46.9 nm [7] was successfully demonstrated by our research group in 2016 and 2022, respectively, utilizing discharge-produced plasma as the gain medium and a SiC mirror as the reflector. Owing to the high hardness of SiC, no appreciable decrease in reflectance was observed after 100 shots of plasma bombardments [6]. Accordingly, the dependence of the double-pass amplification of the 46.9 nm laser on the pre-pulse-to-main-pulse delay was investigated by our research group in 2023 [8]. To date, the pulse waveforms of double-pass-amplified EUV lasers have been primarily investigated by research groups worldwide, and the pulse duration of double-pass-amplified lasers has been observed to be markedly longer than that of single-pass-amplified lasers [1–4]. However, experimental investigations into the beam profiles of double-pass-amplified EUV lasers remain

comparatively scarce. To date, experimental results concerning the spatial intensity distributions of double-pass-amplified lasers have been reported primarily by the Czech group for the Ne-like Zn laser at 21.2 nm [1, 9, 10] and by our research group for the Ne-like Ar lasers at 46.9 nm [7, 8] and 69.8 nm [6]. It is experimentally demonstrated that the poor spatial symmetry of the laser-produced plasma results in irregularly shaped and poorly symmetric beam profiles for both single-pass- and double-pass-amplified EUV lasers [1, 9, 10]. In contrast, owing to the cylindrical geometry of the discharge plasma, the beam profiles of the single-pass- and double-pass-amplified EUV lasers generated thereby exhibit improved spatial symmetry [7, 8].

To date, investigations of the 72.6 nm laser have been conducted exclusively by our research group. In 2011, 72.6 nm laser output was first achieved through single-pass amplification in a discharge-produced plasma [11]. In 2016, using a main-pulse current amplitude of 12 kA, the dependence of the single-pass amplified 72.6 nm laser intensity on the initial gas pressure was investigated [12], and the gain coefficient was determined to be 0.22 cm^{-1}, substantially lower than that of the 69.8 nm laser (0.41 cm^{-1}). In 2022, with the amplitude of the main-pulse current increased to 17 kA, the dependence of the intensity of the single-pass-amplified 72.6 nm laser on the initial gas pressure, pre-pulse current amplitude, and pre-pulse-to-main-pulse delay was investigated [13].

Given the insufficient depth of research on the spatial intensity distribution of double-pass amplified lasers and the fact that double-pass amplification at 72.6 nm has not yet been realized, this study employs a discharge-produced plasma as the gain medium and a SiC mirror to achieve double-pass amplification of Ne-like Ar 69.8 nm and 72.6 nm lasers, and investigates the dependence of the spatial intensity distribution on the initial gas pressure. This work is conducive to enhancing the energy of Ne-like Ar 69.8 nm and 72.6 nm lasers. Furthermore, the experimental results obtained herein offer deeper insight into the influence of plasma conditions on the laser, thereby establishing a foundation for the further enhancement of laser energy in future studies.

2. Experimental setup

The experimental setup for the discharge-produced-plasma EUV laser used in this work has been described in detail in Refs. [14] and [15]. A combined pre-pulse and main-pulse discharge scheme is employed in this setup. The main-pulse power supply is composed of a Marx generator, a Blumlein transmission line, and a main switch. A 200 kV high-voltage pulse generated by the Marx generator is used to charge the Blumlein transmission line. After temporal compression of this pulse by the Blumlein transmission line, the high-voltage pulse is discharged through the initial plasma within the capillary. The main-pulse current waveform is shown in Fig. 1, with a current amplitude of 11.8 kA, a 10%-90% rise time of 33 ns, and a pulse width (FWHM) of 71 ns. In the experiment, an Al_2O_3 ceramic capillary with a length of 35 cm, an outer diameter of 20 mm, and an inner diameter of 3.2 mm was used. An RLC overdamped oscillatory circuit is employed in the pre-pulse power supply, and its circuit diagram and waveform are described in detail in Ref. [15]. The pre-pulse voltage is 20 kV, and the pre-pulse current amplitude is 20 A. In the experiment, the capillary was first filled with Ar gas, and the Ar gas was then broken down by a

high-voltage pre-pulse to form an initial plasma. After a delay of 6 μs, the main-pulse current was passed through the initial plasma, thereby inducing a Z-pinch process. When the plasma is pinched to near its minimum diameter, it contains a high abundance of Ne-like Ar ions, which are excited by electron impact to the upper laser level $2p^5 3p$. When population inversion is achieved between the upper laser level $2p^5 3p$ and the lower laser level $2p^5 3s$, EUV laser output is obtained.

Since both $2p^5 3p$ and $2p^5 3s$ configurations contain multiple sublevels, transitions between different sublevels can simultaneously generate multi-wavelength laser emission at 46.9 nm, 69.8 nm, and 72.6 nm [11, 12]. As shown in Fig. 2, to avoid mutual interference among the lasers at different wavelengths, a spatially resolved flat-field EUV spectrometer was used in the experiments to measure the spatial intensity distributions of the 69.8 nm and 72.6 nm lasers. The EUV laser output from the capillary was collected by a toroidal mirror, and dispersed by a varied-line-spacing grating, and was then imaged onto a CCD (Andor Newton DO920P-BN), thereby enabling the spatial intensity distribution of each laser wavelength along the slit direction to be measured. For the double-pass amplification experiments, a precision-polished SiC mirror was mounted at one end of the capillary and at a distance of 2.5 cm from the plasma column, to reflect the 69.8 nm and 72.6 nm lasers back into the plasma column for a second amplification pass. The reflectance of the SiC mirror at the two wavelengths was measured to be approximately 40%.

3. Experimental results and discussion

According to the experimental results reported in Ref. [14], for a main-pulse current amplitude of 12 kA, the 69.8 nm and 72.6 nm laser intensities are maximized at an initial Ar gas pressure of 16 Pa. Therefore, comparative measurements of the single-pass and double-pass amplified laser intensities at 69.8 and 72.6 nm were first carried out at an initial gas pressure of 16 Pa in this work. The time-integrated spectrum of the plasma radiation measured in the experiments is presented in Fig. 3. It can be seen from Fig. 3, compared with single-pass amplification, the intensities of both the 69.8 and 72.6 nm lasers are markedly enhanced under double-pass amplification, with the intensities of the 69.8 nm and 72.6 nm lasers being 7.4 and 3.5 times those obtained under single-pass amplification, respectively. According to Ref. [6], when a 35 cm-long capillary is used, the length of the gain medium for the 69.8 nm laser has already approached the critical length for gain saturation. Therefore, it can be inferred that the 69.8 nm laser has reached gain saturation under double-pass amplification. By contrast, gain saturation is presumed not to have been reached for the 72.6 nm laser. However, compared with single-pass amplification, double-pass amplification yields a larger intensity enhancement factor for the 69.8 nm laser than for the 72.6 nm laser, indicating that the gain coefficient at 72.6 nm is considerably lower than that at 69.8 nm. This observation is consistent with the gain-coefficient measurements for the two lasers reported in Ref. [12]. Furthermore, according to Ref. [11], the 69.8 nm laser originates from the $3p^3P_2$-$3s^1P_1$ transition, whereas the 72.6 nm laser originates from the $3p^3D_2$-$3s^3P_1$ transition. Because these two transitions involve different upper and lower laser levels, no competition exists between the two laser transitions.

For an initial Ar gas pressure of 16 Pa, corresponding to the condition in Fig. 3, the spatial intensity distributions of the 69.8 nm and 72.6 nm lasers are presented in Fig. 4. As shown in Fig. 4, for the 69.8 nm laser, the beam divergence angle increases from approximately 0.5 mrad under single-pass amplification to approximately 3.3 mrad under double-pass amplification. In contrast, for the 72.6 nm laser, the corresponding divergence angle increases from approximately 0.5 mrad to 3.5 mrad. For both the 69.8 nm and 72.6 nm lasers, appreciable amplification of the feedback radiation reflected back into the gain medium by the SiC mirror was achieved at both the center and the edge of the beam profile, with more pronounced amplification occurring at the edge. According to the theoretical results in Ref. [16], radial variation of the plasma electron density induces refraction during laser propagation and amplification within the plasma, and this refraction becomes more pronounced as the electron density gradient increases. A comparison of the single- and double-pass amplified intensity distributions in Fig. 4 reveals that, there is one component of the feedback light from the SiC mirror, which has relatively small angle with respect to the optical axis. Therefore, this component experiences a relatively small variation in electron density during its propagation in the plasma and is therefore only weakly affected by the refractive effect. After amplification, this component is distributed near the center of the beam profile. For the remaining portion of the feedback radiation, which has a relatively large angle with respect to the optical axis, a relatively large electron density variation is experienced during propagation. As a result, the refractive effect becomes pronounced, leading to its distribution at the periphery of the beam profile after amplification.

Variations in the initial gas pressure are shown to induce changes in the Z-pinch process of the plasma. When the main-pulse current remains constant, the radially inward magnetic pressure exerted on the plasma by the self-generated magnetic field of the high current remains constant. When the initial gas pressure is reduced, the kinetic pressure directed toward the capillary wall within the plasma decreases, thereby accelerating the Z-pinch process. Conversely, when the initial gas pressure is increased, the Z-pinch process proceeds more slowly. Based on the above analysis, variations in the initial gas pressure directly influence the Z-pinch process, thereby affecting the radial distribution of the plasma electron density during laser generation. In the experiment, the initial gas pressure was varied to investigate its effects on the spatial intensity distributions of the 69.8 nm and 72.6 nm lasers under single-pass and double-pass amplification. When the initial argon gas pressure was reduced from 16 Pa (Fig. 4) to 14 Pa, the spatial intensity distributions of the 69.8 nm and 72.6 nm lasers were shown in Fig. 5. As shown in Fig. 5, the beam divergence angle of the 69.8 nm laser increases from approximately 0.5 mrad under single-pass amplification to approximately 2.1 mrad under double-pass amplification, and the corresponding beam divergence angle of the 72.6 nm laser increases from approximately 0.5 mrad to 1.7 mrad. Compared with the case in Fig. 4, a reduction in the gas pressure still resulted in pronounced double-pass amplification near the center of the beam profile, while the intensity amplification at the periphery was markedly weakened. Consequently, the divergence angle of the double-pass-amplified laser at 14 Pa was considerably smaller than that at 16 Pa. In Fig. 5, the amplification at the center of the double-pass-amplified beam profile is more pronounced than that at the periphery, indicating that when the gas pressure is reduced, the radial electron density gradient of the plasma decreases

correspondingly and the refraction of the feedback light by the plasma is weakened, so that after propagation and amplification the feedback light is predominantly distributed near the center of the laser beam profile.

When the initial argon gas pressure was increased from 16 Pa (the pressure used in Fig. 4) to 18 Pa, the spatial intensity distributions of the 69.8 nm and 72.6 nm lasers are shown in Fig. 6. It can be observed from Fig. 6 that the single-pass-amplified beam profiles of the 69.8 nm and 72.6 nm lasers no longer appear as central bright spots with very small divergence angles, whereas the double-pass-amplified beam profiles exhibit a distinct annular structure. Under double-pass amplification, the annular beam profile of the 69.8 nm laser has a peak-to-peak divergence angle of approximately 3.5 mrad, while that of the 72.6 nm laser has a peak-to-peak divergence angle of approximately 3.4 mrad. Compared with the case in Fig. 4, an increase in gas pressure resulted in the amplified feedback light being distributed predominantly at the periphery of the beam profile, which is attributable to the increased radial electron density gradient of the plasma at higher gas pressure and the consequently more pronounced refractive effect.

Comparison of Fig. 4, Fig. 5, and Fig. 6 reveals that, as the initial gas pressure increases, the double-pass-amplified beam profile gradually transforms from a structure with a relatively small divergence angle and a relatively strong central intensity into an annular structure with a relatively weak central intensity. According to the above analysis, this behavior is primarily attributed to the increase in the radial electron density gradient of the plasma at the time of lasing with increasing initial gas pressure, which results in a more pronounced refractive effect on the radiation fed back by the mirror during its propagation in the plasma. The observation that a relatively small variation in the initial gas pressure nevertheless gives rise to a pronounced change in the double-pass-amplified beam profile. This phenomenon indicates that the 69.8 nm and 72.6 nm lasers are highly sensitive to variations in the plasma conditions, which also constitutes the primary reason why they are difficult to observe experimentally.

4. Conclusion

With a high-temperature, high-density plasma produced by a high-current Z-pinch as the gain medium, EUV lasers at 69.8 nm and 72.6 nm were achieved via energy-level transitions of Ne-like Ar ions. By employing a SiC mirror to provide optical feedback, the laser was reamplified during a second pass through the plasma, and double-pass amplification of the EUV lasers at 69.8 nm and 72.6 nm were achieved. The experimental results demonstrate that the intensities of the double-pass amplified 69.8 nm and 72.6 nm lasers were enhanced by factors of 7.4 and 3.5 compared with those under single-pass amplification at an initial gas pressure of 16 Pa, respectively. A flat-field grating spectrometer was employed to measure the spatial intensity distribution of the laser along the slit direction of the spectrometer. The effects of the initial gas pressure on the double-pass amplified lasers were experimentally investigated. The results indicate that, with increasing gas pressure, the influence of refraction on the feedback beam during its propagation and amplification in the plasma becomes

progressively more pronounced. The double-pass-amplified beam profile gradually evolves from a central-intensity-dominated profile at low gas pressure into an annular profile. Since the radial electron density gradient is the primary parameter determining the refraction angle of light, it can be inferred from the spatial intensity distribution of the double-pass amplified laser that the radial electron density gradient of the plasma at the time of laser generation tends to increase with increasing gas pressure. The dependence of the spatial intensity distribution of the laser on the initial gas pressure obtained in this work lays the foundation for further enhancing the energy of the 69.8 nm and 72.6 nm lasers, and for future multi-pass amplification using a resonant cavity.

Declarations

Author contributions Yongpeng Zhao: conceived the idea; Yongpeng Zhao and Huaiyu Cui: review and supervision; Shuisen Jiang and Tao Liu: conducted experiments; Shuisen Jiang, Tao Liu and Dongdi Zhao: analyzed data and wrote the manuscript; all authors have read and agreed to the submitted version of the manuscript.

Funding National Natural Science Foundation of China (61875045). Natural Science Foundation of Fujian Province (2026J001966).

Conflict of interest The authors declare no conflicts of interest.

References

1. B. Rus, T. Mocek, A.R. Prag, M. Kozlova, G. Jamelot, A. Carillon, D. Ros, D. Joyeux, D.P. Multimillijoule, Phys. Rev. A **66**, 063806 (2002)
2. N.M. Ceglio, D.P. Gaines, D.G. Stearns, A.M. Hawryluk, Opt. Commun. **69**, 285 (1989)
3. A. Carillon, H.Z. Chen, P. Dhez, L. Dwivedi, J. Jacoby, P. Jaegle, G. Jamelot, J. Zhang, M.H. Key, A. Kidd, A. Klisnick, R. Kodama, J. Krishnan, C.L.S. Lewis, D. Neely, P. Norreys, D. O'Neill, G.J. Pert, S.A. Ramsden, J.P. Raucourt, G.J. Tallents, J. Uhomoibhi, Phys. Rev. Lett. **68**, 2917 (1992)
4. S.T. He, S.T. Chunyu, Q.R. Zhang, A. He, H.Z. Shen, Y.L. Ni, S.Y. Yu, Phys. Rev. A **46**, 1610 (1992)
5. J.J. Rocca, D.P. Clark, J.L.A. Chilla, V.N. Shlyaptsev, Phys. Rev. Lett. **77**, 1476 (1996)
6. Y.P. Zhao, T. Liu, W.H. Zhang, W. Li, H.Y. Cui, Opt. Lett. **41**, 3779 (2016)
7. Y.P. Zhao, D.D. Zhao, B. An, L. Li, Y.S. Bai, H.Y. Cui, Opt. Commun. **506**, 127571 (2022)
8. D.D. Zhao, Y.P. Zhao, H.Y. Cui, B. An, L. Li, Y.S. Bai, Chin. Opt. Lett. **21**, 53401 (2023)
9. A.R. Prag, T. Mocek, M. Kozlova, B. Rus, G. Jamelot, D. Ros, Eur. Phys. J. D **22**, 31 (2003)
10. T. Mocek, B. Rus, A.R. Prag, M. Kozlova, G. Jamelot, A. Carillon, D. Ros, J. Opt. Soc. Am. B **20**, 1386 (2003)
11. Y.P. Zhao, S. Jiang, Y. Xie, D. Yang, S. Teng, D. Chen, Q. Wang, Opt. Lett. **36**, 3458 (2011)
12. Y.P. Zhao, T. Liu, S. Jiang, H.Y. Cui, Y.J. Ding, L.B. Li, Appl. Phys. B **122**, 107 (2016)

13. Y.S. Bai, Y.P. Zhao, B. An, D.D. Zhao, H.Y. Cui, L. Li, J.Q. Li, Appl. Phys. B **128**, 163 (2022)
14. Y.P. Zhao, Y.L. Cheng, B.H. Luan, Y.C. Wu, Q. Wang, J. Phys. D: Apply Phys. **39**, 342 (2006)
15. S. Jiang, Y.P. Zhao, Y. Xie, M. Xu, H.Y. Cui, H. Wu, Y. Liu, Q. Xu, Q. Wang, Appl. Phys. B **109**, 1 (2012)
16. Y.P. Zhao, D.D. Zhao, Q. Yu, M.U. Khan, H.Q. Lu, J.J. Li, H.Y. Cui, J. Opt. Soc. Am. B **37**, 2271 (2020)

Figures

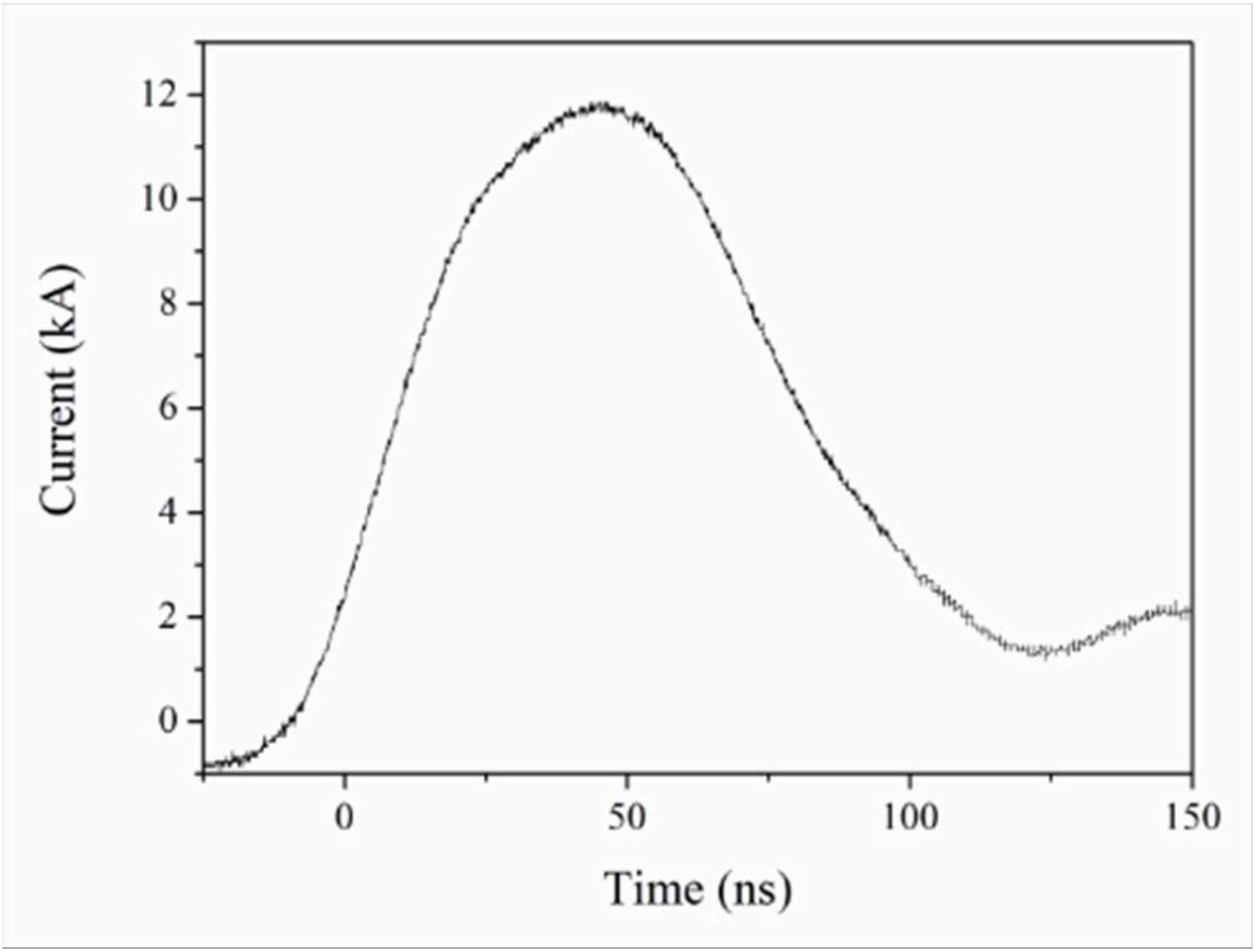


Figure 1

Typical current waveform of main pulse

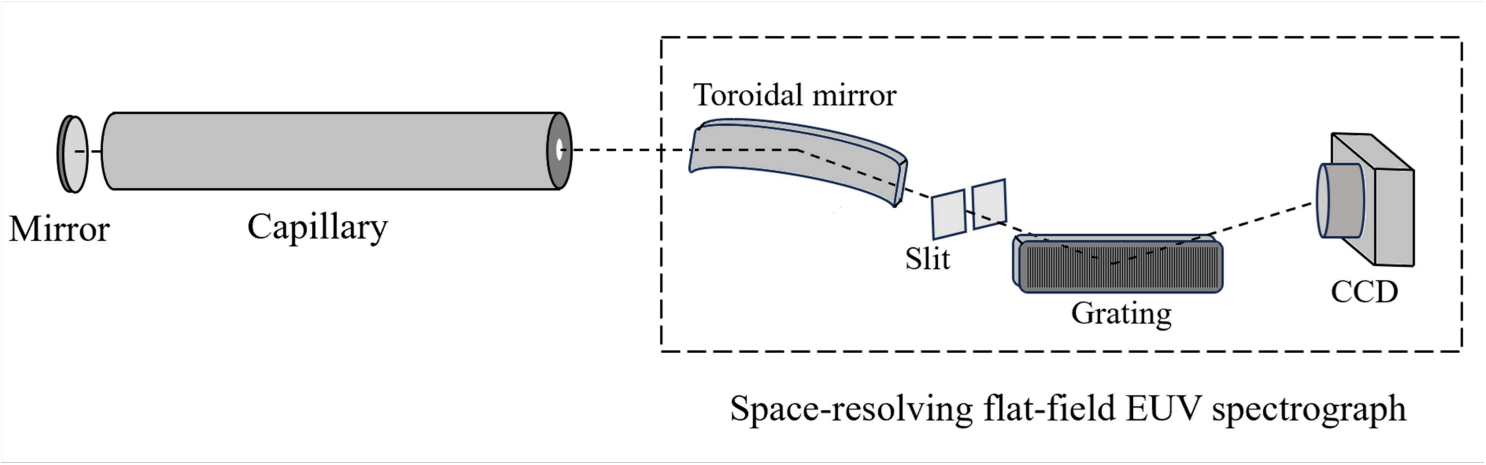


Figure 2

Schematic diagram of the experimental setup

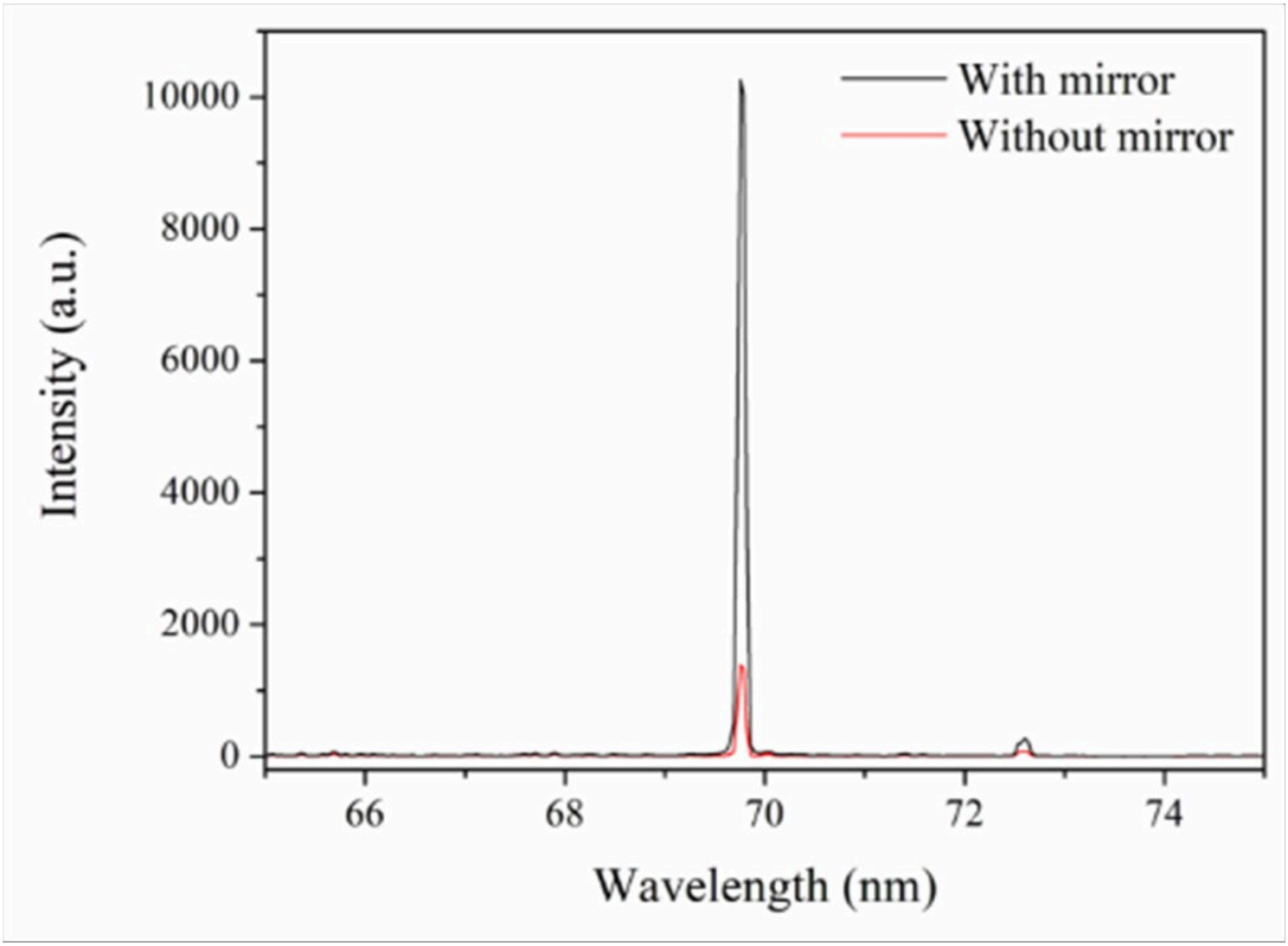
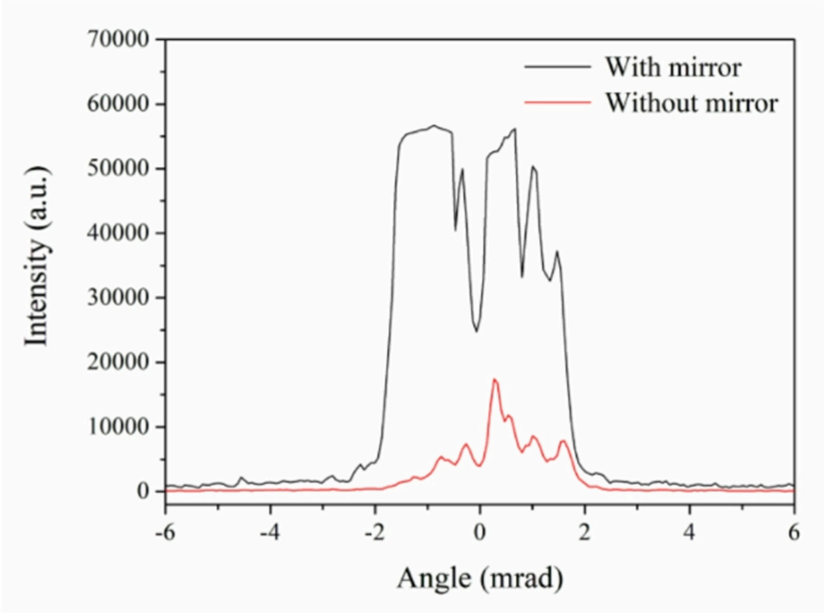
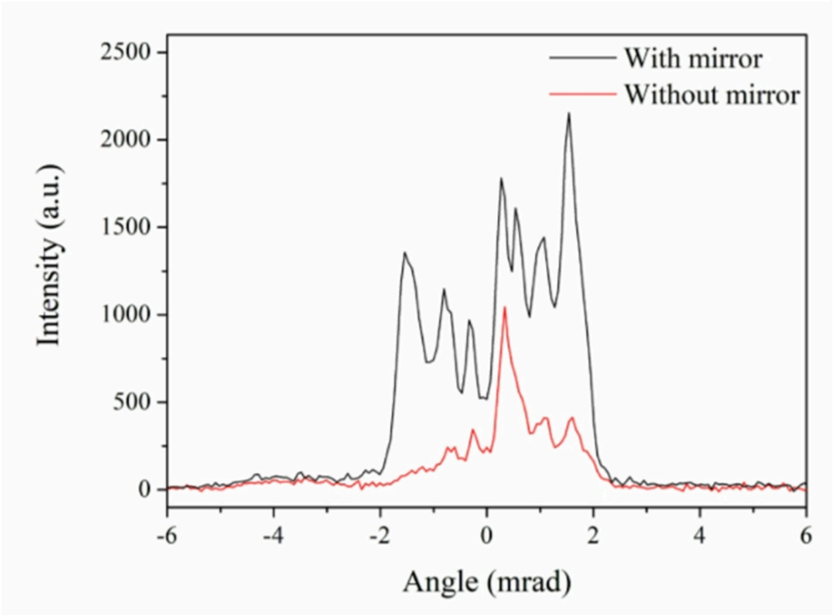


Figure 3

Time-integrated spectrum of plasma emission



(a)



(b)

Figure 4

Spatial intensity distributions of single-pass and double-pass amplified extreme ultraviolet lasers at an initial gas pressure of 16 Pa

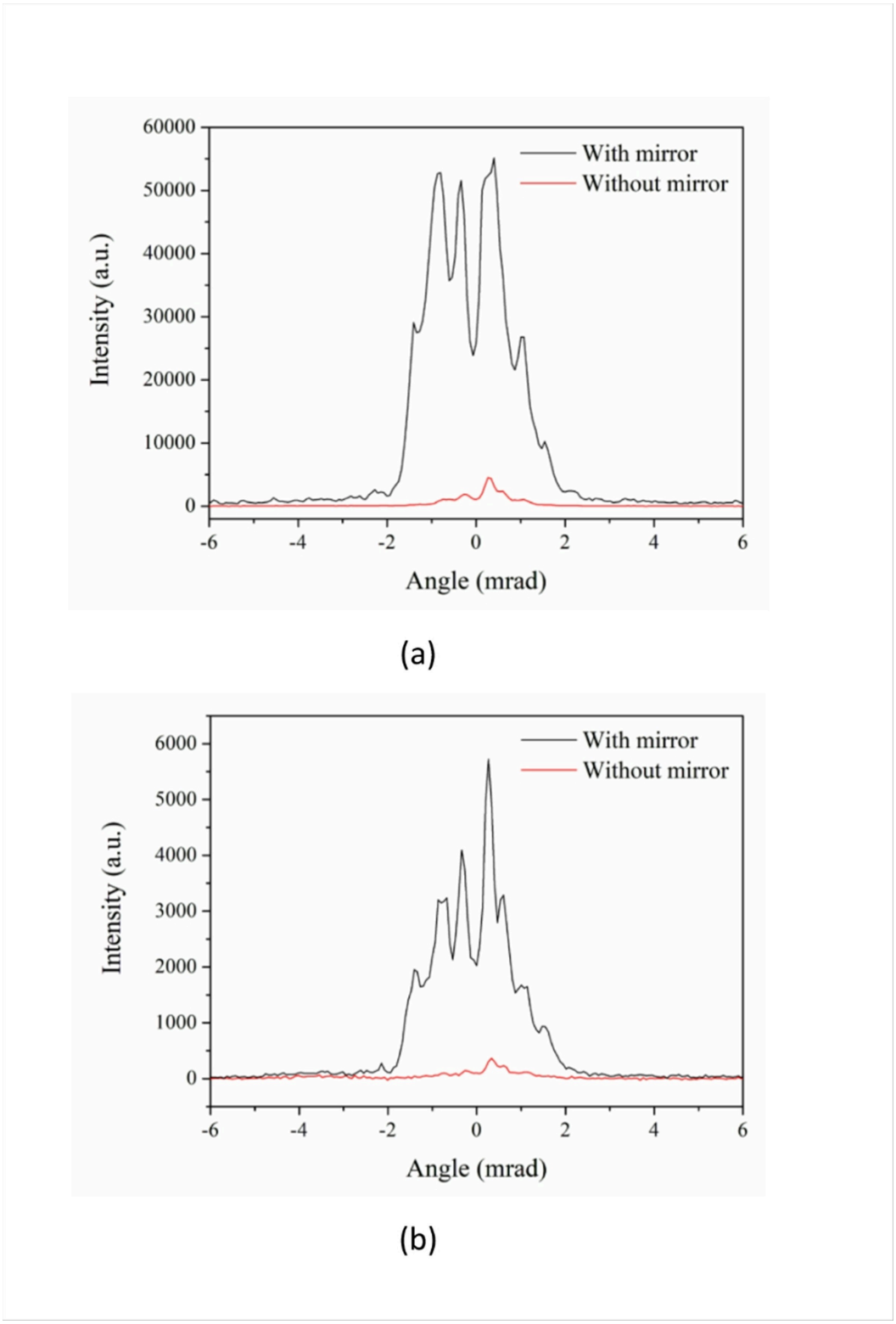
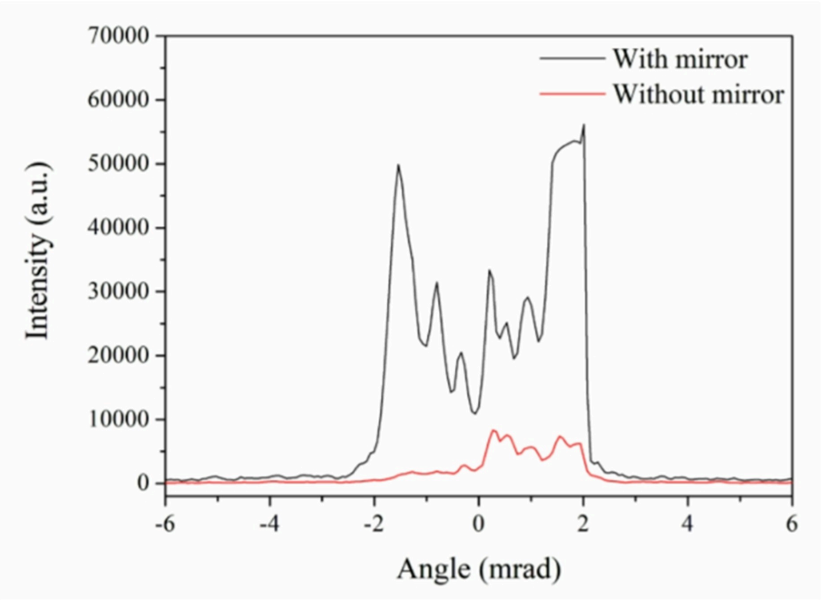
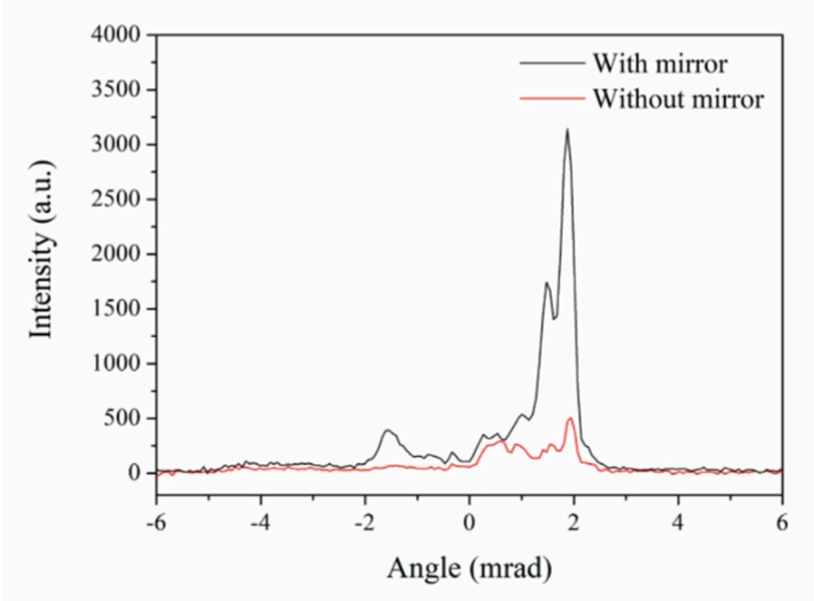


Figure 5

Spatial intensity distributions of single-pass and double-pass amplified extreme ultraviolet lasers at an initial gas pressure of 14 Pa



(a)



(b)

Figure 6

Spatial intensity distributions of single-pass and double-pass amplified extreme ultraviolet lasers at an initial gas pressure of 18 Pa